DESIGN AND SIMULATION OF NON-CRIMP FABRIC CARBON FIBER/EPOXY CHANNELS FOR ENERGY ABSORBING APPLICATIONS

Pravin Gopal Samy Dharmaraj[1], Jeffrey Wood[2], John Montesano[1]
[1] Department of Mechanical & Mechatronics Engineering, University of Waterloo, 200 University Avenue West, Waterloo N2L 3G1, Canada
[2] Department of Mechanical and Materials Engineering, Western University, Spencer Engineering Building, London N6A 5B9, Canada

Abstract

Owing to their high specific properties and inherent energy absorption characteristics, carbon fiber-reinforced plastics (CFRP) may be suitable alternatives for replacing metallic components in front-end automotive structures. Straight CFRP channels used as main frontal crush rails are likely to fail progressively by splaying or widespread fragmentation, including local matrix cracking and fiber breakage, which comprise their main energy absorption mechanisms. In this study, a numerical simulation approach was used to investigate the response of unidirectional non-crimp CFRP laminated crush rails under dynamic impact conditions. The specific energy absorption capabilities of four CFRP channels with variable cross-sections are compared, while the simulation results are used to optimize their design for improving crashworthiness and enhancing CFRP utilization. Specific energy absorption was also predicted for two different stacking sequences, including $[0/\pm45/90]_s$ and $[\pm45/0_2]_s$, where the latter proved to yield higher energy absorption for each channel geometry considered. The results of the study provide important insight for the development of future vehicle CFRP frontal crush structures.

Introduction

Passive safety is an important consideration in the overall design of a vehicle, which may affect the vehicle weight due to the corresponding structural performance requirements and energy management. Advanced composites such as carbon fiber reinforced plastics (CFRP) have superior specific strength and stiffness properties and may be an excellent alternative to conventional metallic structures used in automobiles [1]. In addition, CFRPs have inherent energy absorption characteristics and may be used to replace existing metallic crash structures to improve energy absorption while reducing the overall vehicle mass. Composites exhibit high energy absorption by complex failure mechanisms like splaying and fragmentation, as well as local damage, including matrix cracking and fiber breakage.

Heavy tow Non-Crimp Fabrics (NCF) are a new generation of fabrics which are increasingly considered in automotive structural applications because of their low production costs compared with conventional woven or braided fabrics. By coupling NCFs with an accelerated curing resin and utilizing a high-pressure resin transfer molding (HP-RTM) process, the production of composite parts at high volume rates required for automotive industries may be enabled. Composite parts may be fabricated with cycle times of less than one minute using the HP-RTM process [2-4]. Moreover, unidirectional stitched NCFs specifically designed for resin transfer molding processes provide a balance between required drapability and performance.

One of the most commonly assessed structural components in a vehicle is the front rail, which is a primary energy absorber during front-end collisions. McGregor et al. [5, 6] investigated the axial crush performance and failure characteristics of braided CFRP tube specimens. Deleo et al.

[8] conducted experiments on CFRP square tubes and C channels to examine their progressive failure behavior. Most reported studies have focused on assessing the performance of round and square closed-section composite tubes [8-10] due to their stable geometries. However, in practice front rails typically have two different components joined together to form a closed section, such as a channel and backing plate, as well as additional vehicle components attached along their length, including side reinforcements, a shock tower, and engine components. To incorporate cost-effective fabrication processes such as HP-RTM, multi-component rails would be required. Also, most research on energy absorption of composites was conducted under quasi-static loads, while research comparing static and dynamic performance shows that properties of composites may vary significantly with the loading rate [11-12]. Furthermore, the performance of NCF-based CFRP axial crush rails has not received much attention [13]. Consequently, there is a need to study the axial crush response and failure characteristics of CFRP rails with various section geometries under dynamic loading conditions.

This paper aims to address a current gap in the literature by conducting a thorough numerical study of NCF CFRP channels under dynamic axial crush loads. Axial crush specimens with different geometries and stacking sequences were investigated to determine the corresponding influence on specific energy absorption.

Material Properties and Laminate Stacking sequence

The HP-RTM fabricated material consisting of 8 unidirectional NCF layers and a rapid curing resin with a total laminate thickness of 2.6mm was considered in this study [13]. The mechanical properties of the corresponding lamina extracted from Refs. [13, 18] are shown in Table 1.

Table I: Unidirectional ply properties [13,18]

Mechanical Properties	Value
Longitudinal Young's modulus E1, GPa	102.7
Transverse Young's modulus E2, GPa	8.1
In-plane shear modulus G_{12}, GPa	3.1
Longitudinal tensile strength X_t, MPa	1204.0
Transverse tensile strength Y_t, MPa	51.9
Longitudinal compressive strength X_c, MPa	575.2
Transverse compressive strength Y_c, MPa	150.2
In-plane shear strength S_L, MPa	65.3
Major in-plane Poisson's ratio γ_{12}	0.253
Longitudinal tensile strain at failure ε_{1f}, %	1.175
Transverse tensile strain at failure ε_{2f}, %	0.694
In-plane shear strain at failure γ_{12f}, %	5.357

The relation between the laminate stacking sequence, channel cross-sectional geometry and the subsequent failure modes are difficult to predict because of the potential diversity in the layup sequence. Kalhor et al. [14] and Mahdi et al. [15] found that energy absorption of composites during axial crush are highly influenced by the stacking sequence.

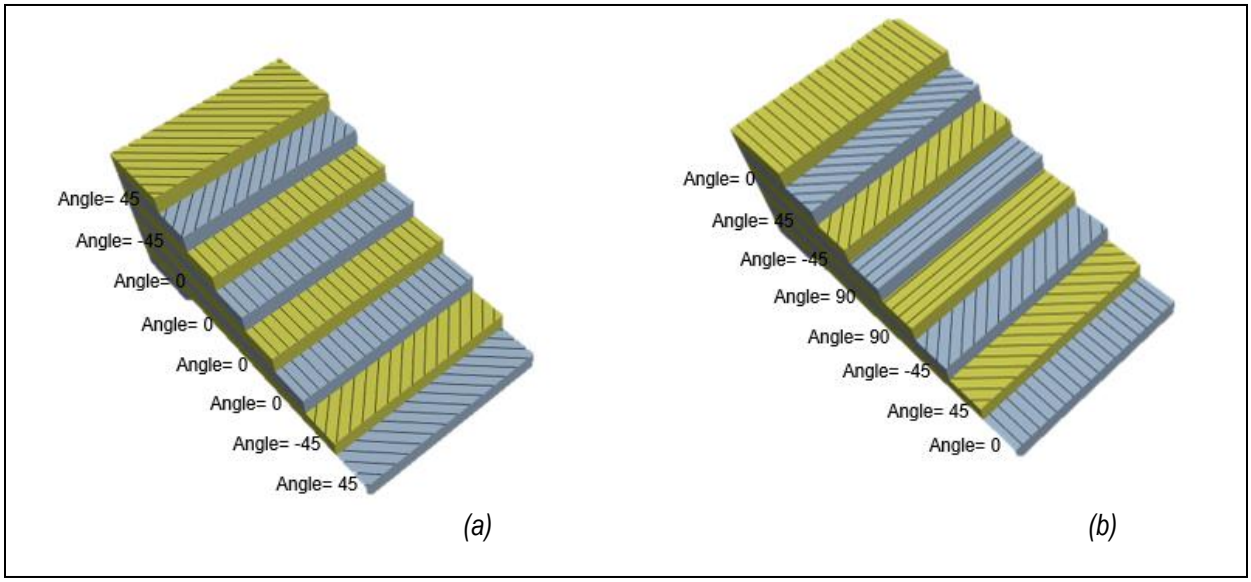

Figure 1: Stacking configuration (a) $[\pm 45/0_2]_s$ (b) $[0/\pm 45/90]_s$

In the current study, the energy absorption of different channels with two stacking sequences were studied. The two laminate stacking configurations analyzed (see Figure 1) are $[\pm 45/0_2]_s$ and $[0/\pm 45/90]_s$ and referred to as layup 1 and 2 respectively. The main differences are the number of 0° and 90° plies oriented towards the channel axis and the position of these plies.

Numerical Model Development

Geometrical variations

In addition to the variable laminate stacking sequence, four sets of geometries (Hat Channel, W Channel, B Channel and Octagon Channel) were designed for the axial crush specimens which had two different components, a CFRP channel and backing plate. The channels and backing plates had an overall length of 400mm and the channels had a cross-section width and height of 200mm and 80mm respectively. Additionally, 15mm flanges were provided on either sides of the channels to bond the axial crush specimens together. The detail dimensions of each axial crush specimen are given in Figure 2.

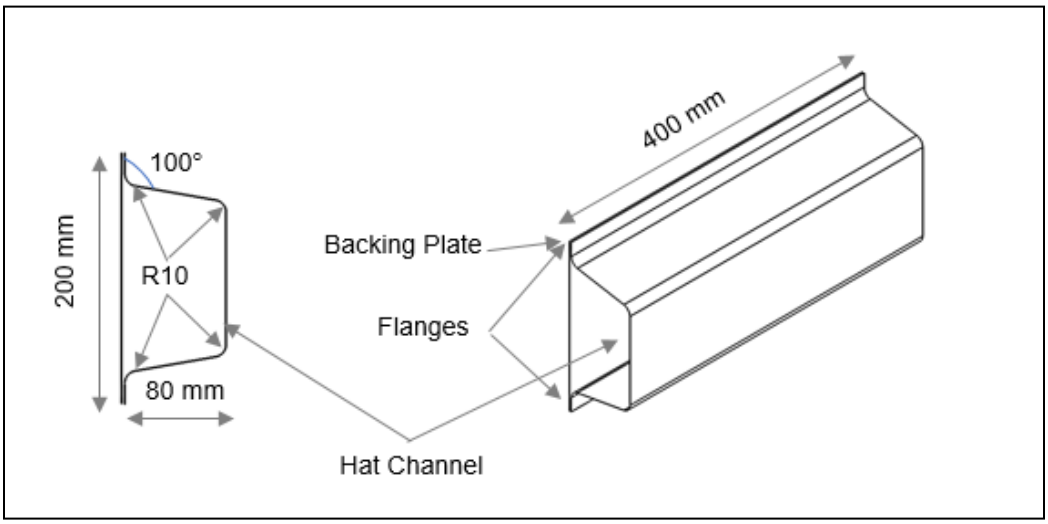
100°
200 mm
R10
80 mm
400 mm
Backing Plate
Flanges
Hat Channel

(a)

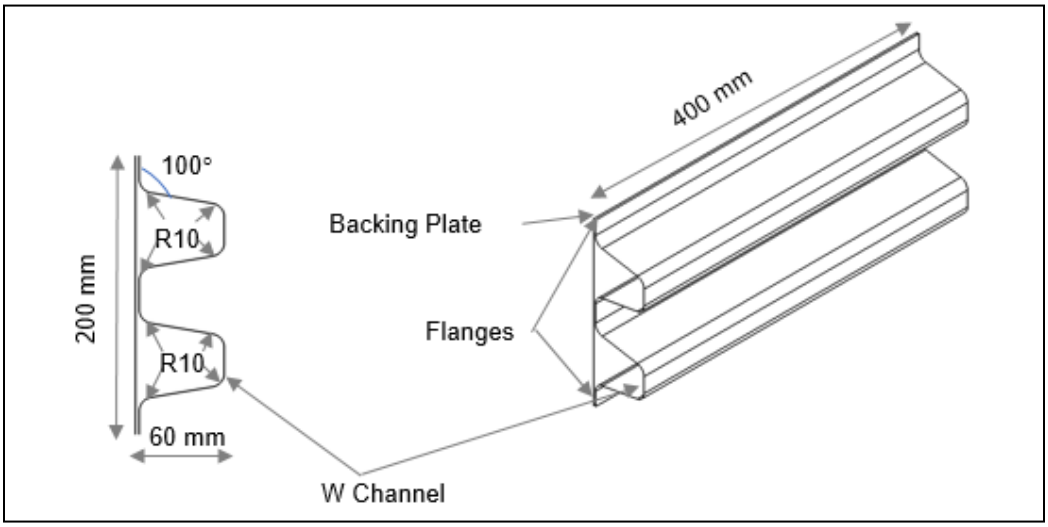
100°
R10
200 mm
R10
60 mm
400 mm
Backing Plate
Flanges
W Channel

(b)

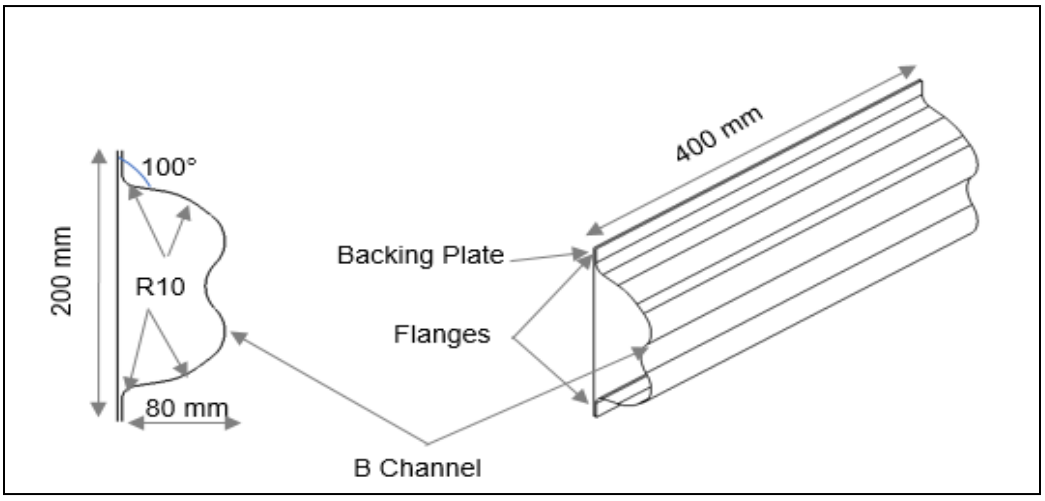
100°
200 mm
R10
80 mm
400 mm
Backing Plate
Flanges
B Channel

(c)

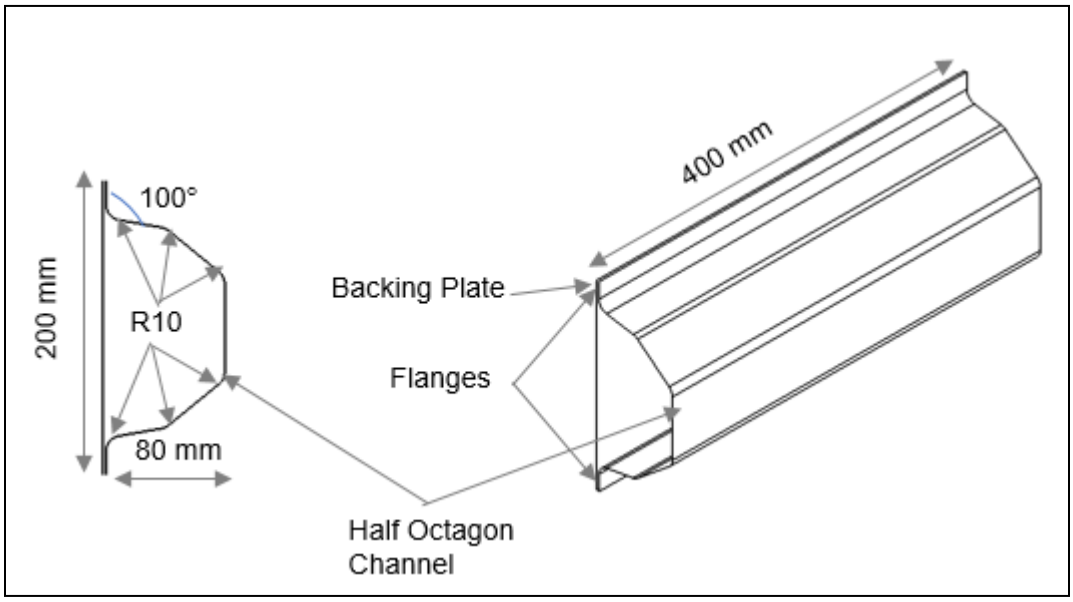

(d)

Figure 2: Dimensions of the CFRP parts (a) Hat Channel (b) W Channel (c) B Channel (d) Octagon Channel

MAT 54 constitutive Model

The dynamic behavior of the axial crush specimens were assessed using the explicit finite element code LS-Dyna, which includes a wide range of pre-existing material models available for simulating the response of composite components. Several studies have examined the correlation and limitations of each model in the LS Dyna [7, 10,16, and 17]. Feraboli et al. [7], Alex et al. [16], Boria et al. [17] investigated the axial crush response of simple structures and concluded that the predictive capabilities of the commonly employed MAT_ENHANCED_COMPOSITE_DAMAGE (*MAT54) has a good correlation with the experimental results. Moreover, the *MAT 54/55 material model is specifically designed to represent orthotropic laminate materials and requires relatively few input properties which can be measured using standard material tests. Also, *MAT 54 utilizes laminate theory with 2D stress assumption and shell elements, which significantly reduces the computational requirements. Thus, *MAT54 was used in this study.

The constitutive model utilizes a progressive failure-based approach which degrades the elastic properties at the lamina level along with failure criteria, while a ply discount approach is used to govern laminate degradation. The failure criteria of this model are governed by Chang-Chang stress-based equations [19], and are defined for each fiber and matrix failure mode as follows:

For Tensile fiber mode

$$e_f^2 = \left(\frac{\sigma_{aa}}{X_t}\right)^2 + \beta\left(\frac{\sigma_{ab}}{S_c}\right)^2 - 1 \quad (1)$$

For Compressive fiber mode

$$e_c^2 = \left(\frac{\sigma_{aa}}{X_c}\right)^2 - 1 \quad (2)$$

For Tensile matrix mode

$$e_m^2 = \left(\frac{\sigma_{bb}}{Y_t}\right)^2 + \left(\frac{\sigma_{ab}}{S_c}\right)^2 - 1 \quad (3)$$

For Compressive matrix mode

$$e_d^2 = \left(\frac{\sigma_{bb}}{2S_c}\right)^2 + \left[\left(\frac{Y_c}{2S_c}\right)^2 - 1\right]\frac{\sigma_{bb}}{Y_c} + \left(\frac{\sigma_{ab}}{S_c}\right)^2 - 1 \quad (4)$$

Here, σ_{ij} are the in-plane stress of a lamina and $e_f^2, e_c^2, e_m^2, e_d^2$ are the failure modes in longitudinal tensile, longitudinal compressive, transverse tensile, and transverse compressive failures. The β parameter is defined as the shear weighting factor in longitudinal tensile mode, while X_t, X_c, Y_t, Y_c and S_c are the lamina longitudinal tensile, longitudinal compressive, transverse tensile, transverse compressive and in-plane shear strengths. The moduli and strength parameter of the lamina are shown in Table 1. In addition to the mechanical properties, a set of non-physical parameters in MAT54 require definition. These parameters are mainly classified into three groups: erosion parameters, crash front softening parameter, and parameters that control the material behavior after failure initiation. For erosion, the parameters minimal time step failure (TFAIL), effective plastic strain (EPS) and directional failure strains (DFAIL_) ensure the elemental deletion never exceeds the physical failure criteria. As the elements are eroded, the strength of the proceeding elements in the crush front are reduced by certain factor which is specified by the SOFT parameter. The post-failure behavior of a composite is controlled by the stress limit factor (SLIM and SLIMC1) parameters, which indicate the amount of residual stress that are retained after compressive loading. A schematic stress-strain curve of MAT54 model is shown in Figure 3.

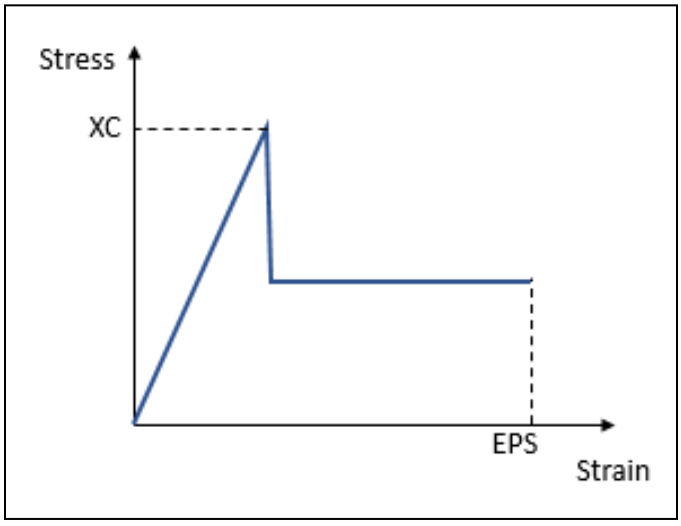

Figure 3: Schematic compressive stress-strain behavior a ply using MAT54 [16]

The values of the non-physical parameters are shown in Table 2 and were previously defined in Reference [16].

Table 2: Non-Physical parameters of MAT54 [16]

Non-Physical Parameters	Value
AOPT	2
TFAIL	1E-7
EPS	0.55
SOFT	0.8
SLIMT1	0.01
SLIMC1	0.375
SLIMT2	0.10
SLIMC2	1.00
SLIMS	1.00
YCFAC	2.00

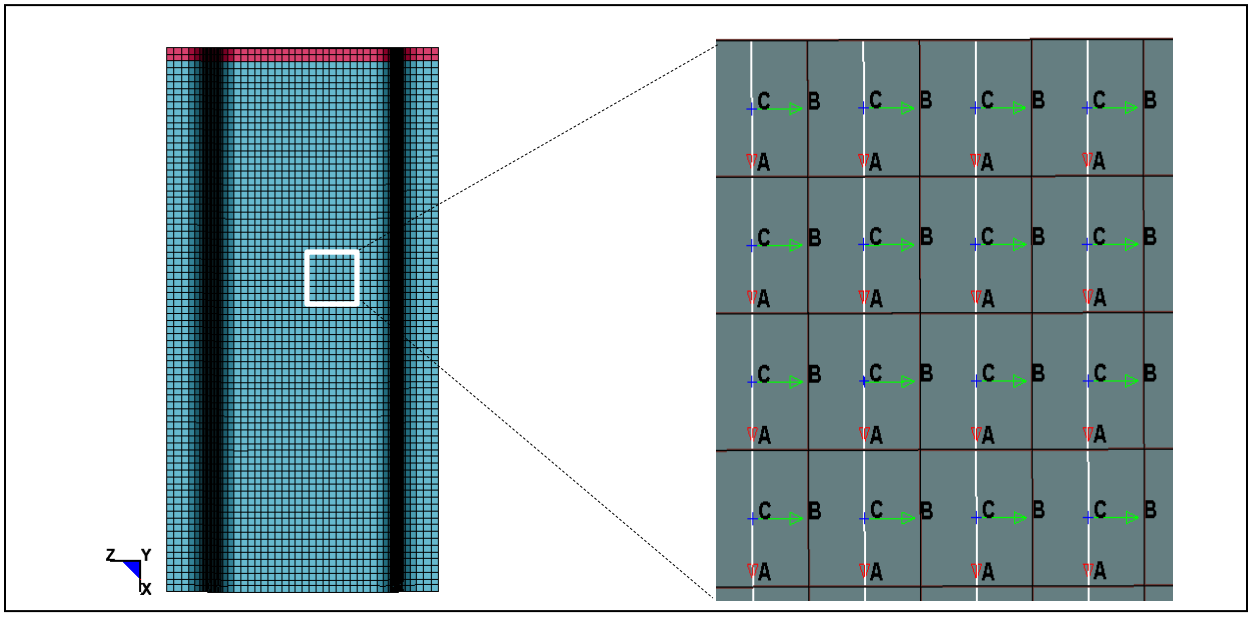

Figure 4: Assigning Principle Material co-ordinates (Hat channel shown)

MAT 54 is formulated at the ply level, such that the lamina properties are the input parameters for the material model. In addition to the ply properties, ply orientation should be provided to assign the principle material axis, which can be specified by the AOPT parameter. In the current study, the parameter was set to 2, which aligned the material coordinates (A, B, C) to the global

coordinates(X, Y, Z) system. The A1, A2, and A3 parameters were set to 1,0,0 to align the A axis with global X direction (as shown in Figure 4), and the other directions are computed based on the inputs provided.

Finite element model

The channels and the backing plate were modeled with a single layer of shell elements of size approximately 5mm x 5 mm, which is a typical size used in industries for automobile crash applications. The elemental formulation of type 16 with fully integrated 4-noded shell elements was considered throughout the study. The composite laminate theory was invoked by setting the LAMSHT flag to 1 in the *CONTROL_SHELL card, which accounts for through-thickness non-uniform shear strain behavior.

When employing shell elements, each integration point through the thickness represents the number of physical plies in the laminate. The *ELEMENTAL_SHELL_COMPOSITE defines the composite layup configuration in which the thickness and orientation of each ply (integration point) were assigned to shell composites. As an example, Figure 5(b) represents the laminate sequence [0/±45/90] or material co-ordinates assigned for each integration point by rotating with respect to the principal material axis.

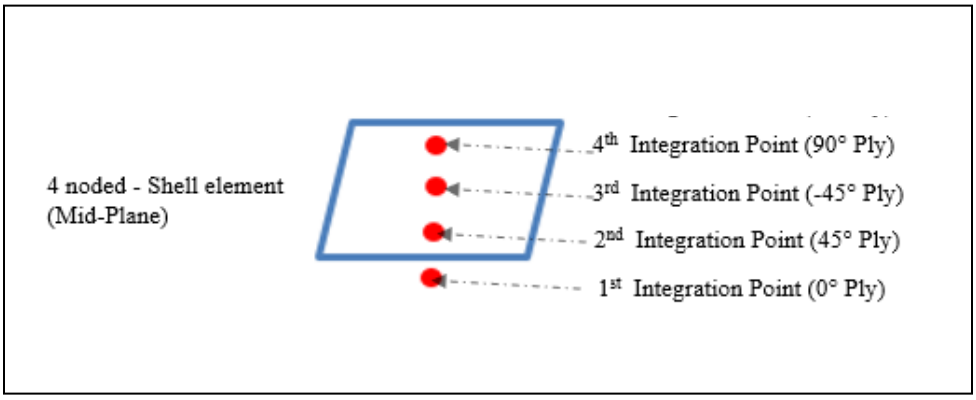

(a)

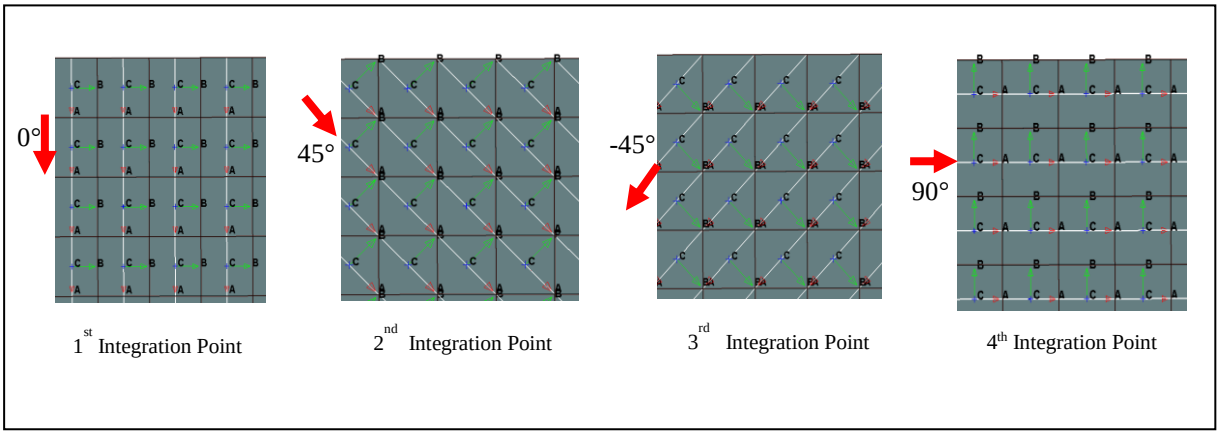

(b)

Figure 5: (a) 2D stress state composite model, (b) Orientation of Material Co-ordinates for [0/±45/90]$_s$.

Figure 6 represents the numerical model which consisted of four parts: channel, backing plate, bevel trigger, and impactor (not shown). The impactor represents a rigid body of mass 855 kg,

which impacted the specimen at one end with a velocity of 7.5 m/s. The other end of the specimen was clamped with a rigid fixture for 50mm length. The bevel trigger was represented with a reduced thickness of 1.3mm to provide a gradual transition between the regular and trigger shell elements. The *CONTACT_AUTOMATIC_SURFACE_SURFACE_TIEBREAK contact was used to define the bonded contact between the channel and backing plate. The *CONTACT_AUTOMATIC_SURFACE_TO_SURFACE with a friction coefficient of 0.2 was established to define contact between the specimen and impactor.

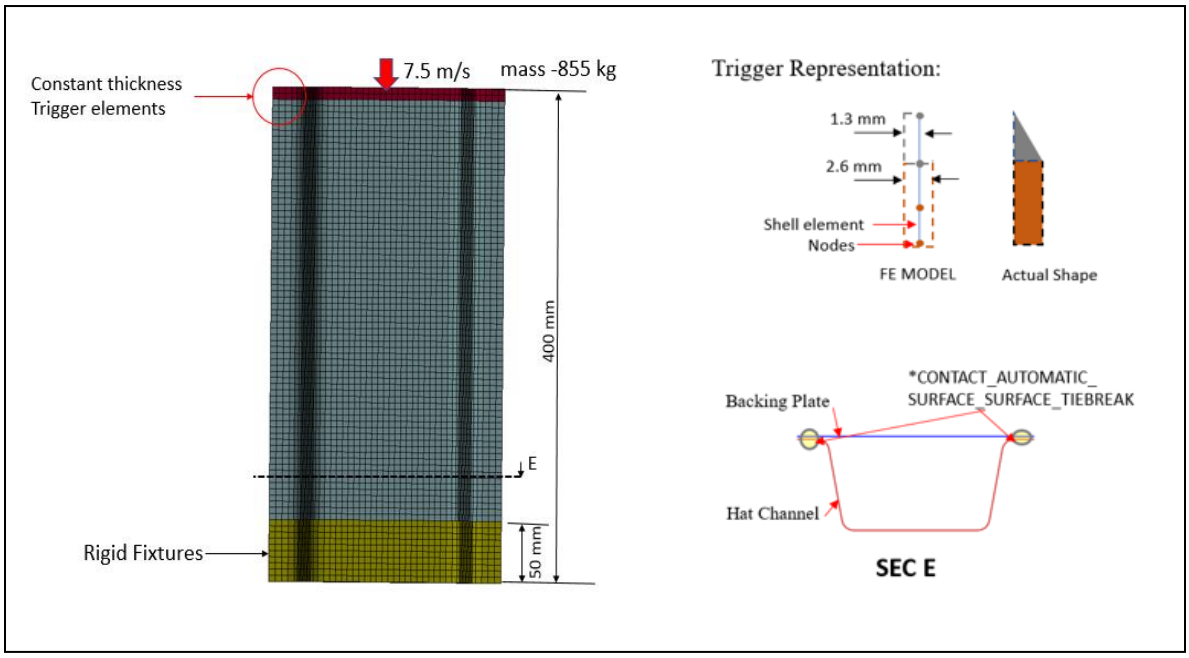

Figure 6: LS Dyna model for axial crush specimen impact simulation (hat channel shown).

Results and Discussion

Crashworthiness metrics

The general aim of the crashworthiness metrics is to evaluate the energy absorbing characteristics of the structure. Figure 7 represents a typical force-displacement curve for a component under axial crush loading.

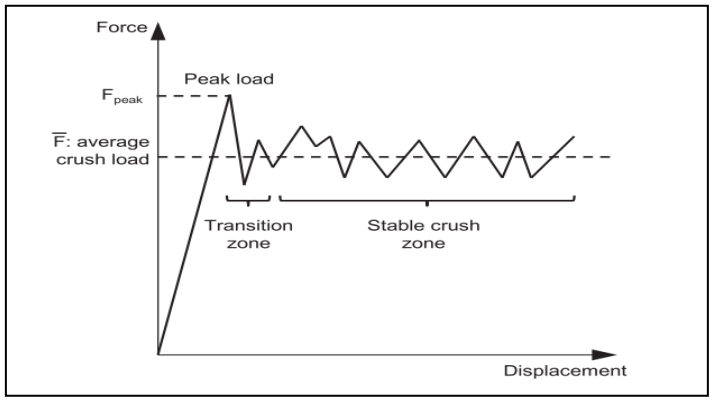

Figure 7: Typical Force-displacement curve [20].

Crashworthiness of structures can be evaluated by several parameters, such as peak force, mean crush force, total energy absorption, and specific energy absorption. The peak force (F_{peak}) is the critical parameter that represents the high force experienced during the initial crushing, which potentially increases the possibility of injury to the occupants. The stable or mean crush force can be analytically formulated as displacement average of force history, and defined by:

$$\boldsymbol{F_{mean} = \frac{\int Fdl}{l}} \quad (5)$$

Here, *l* represents the length of the axial crush specimen or structure. The energy absorption (EA) of a structure is calculated from the total area under the force-displacement curve. Specific Energy absorption is the second most critical index for axial crush specimen, which is energy absorbed per unit mass of the crushed structure.

$$\boldsymbol{EA = \int Fdl} \quad (6)$$

$$\boldsymbol{SEA = \frac{EA}{m}} \quad (7)$$

Here, m is the mass of the crash structure.

Overview of $[\pm 45/0_2]_s$ laminate in different cross sections

Figure 8 presents the collapse of four axial crush channels. As can be seen, all channels developed the same failure mode known as fragmentation, in which fronds of the material are formed. This is in contrast to the more ductile concertina folding deformation found in metallic structures. During crushing of the specimens, these fronds move outward promoting tearing of the elements at the corners of the specimens. In this way, more energy is absorbed in the corner by large deformation comparing to the elements located in fronds.

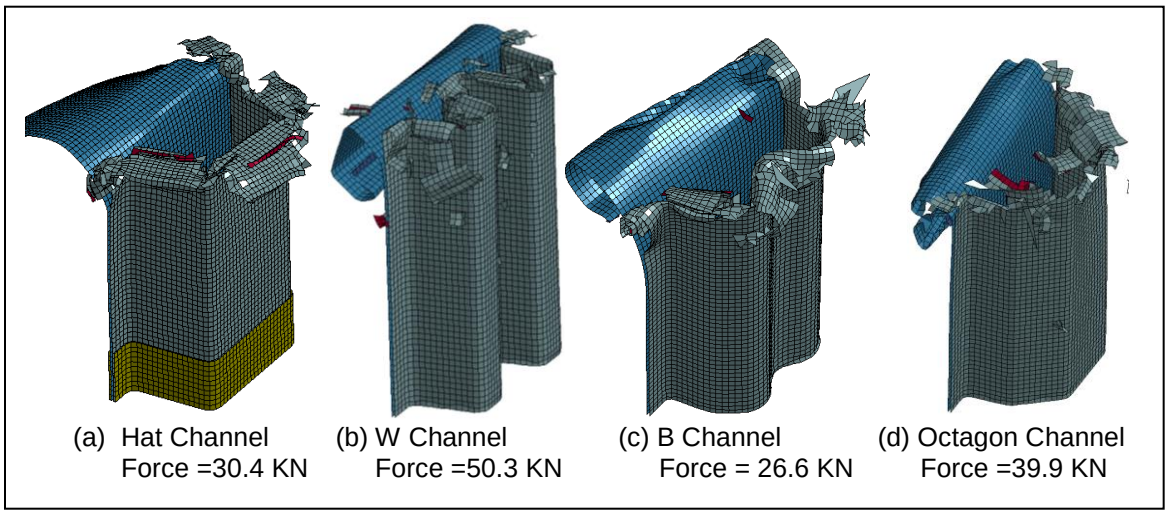

Figure 8: Layup 1 – failure modes in different cross sections at 150 mm displacement (At time, t =20 ms).

Figure 9 presents the force-displacement curves for the four axial specimens designed with a $[\pm 45/0_2]_s$ layup sequence. The initial peak load for all the channels occurred between 10 – 15 mm of vertical displacement up to a maximum force of 70 – 95 KN, after which the crushing load was stabilized with some oscillations until full failure of the specimens. The several peaks before the

peak force were a result of the trigger elements, which were intended to reduce the force peaks and ensure the stable crushing. In particular, two different wall thickness zones were designed for the trigger along the longitudinal axis; 1.3mm and 2.6mm respectively, as shown in Figure 6. Progressive reduction of wall thickness from back to front, which reduces the resisting section locally to have low impact force.

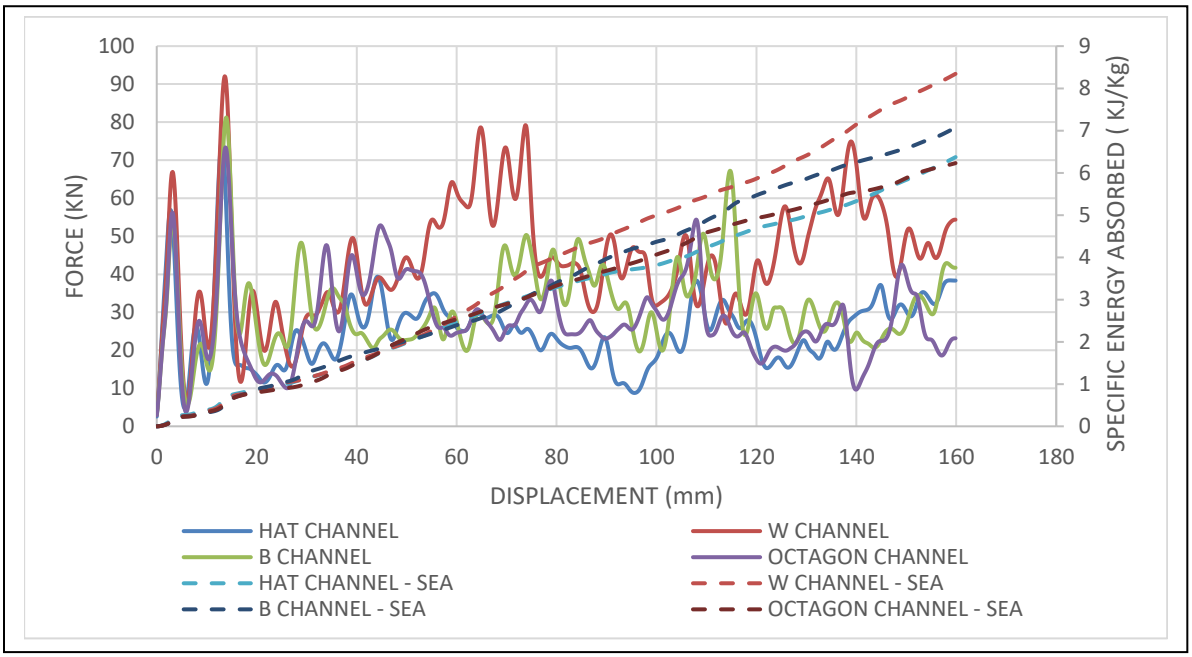

Figure 9: Layup 1 - force-displacement and specific energy absorption plots

Overview of $[0/\pm45/90]_s$ laminate in different cross sections

Figure 10 shows the laminate failure behavior with $[0/\pm45/90]_s$ layup sequence. Presence of 90° plies in the center, triggers progressive crushing by the propagation of local cracks which split the specimen into external and internal fronds. Some fronds from the corner and straight areas broke off entirely from the crushed specimen, and formed smaller pieces of debris in all the axial crush specimens. From the force-displacement plots in Figure 11, it can be seen that the initial peak force for all the specimens was between 65 - 90 KN. The same trend of load-displacement curves was interpreted, maintaining two initial peaks, which was developed due to the varying thickness and stable crushing until the estimated vertical displacement. Similarly, It can be concluded that gradual reduction of force-displacement plots was observed in $[0/\pm45/90]_s$ stacking sequence, which is due to the fact that unstable buckling mode occurs during crushing led to relatively low load carrying capacity.

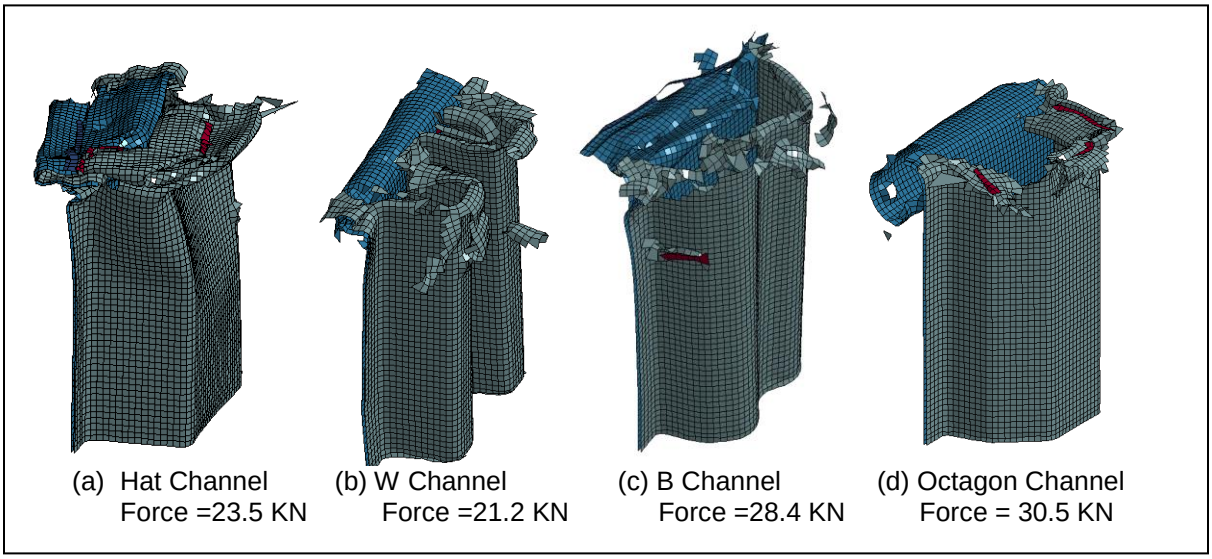

Figure 10: Layup 2 – failure modes in different cross sections at 150 mm displacement (At time, t = 20 ms).

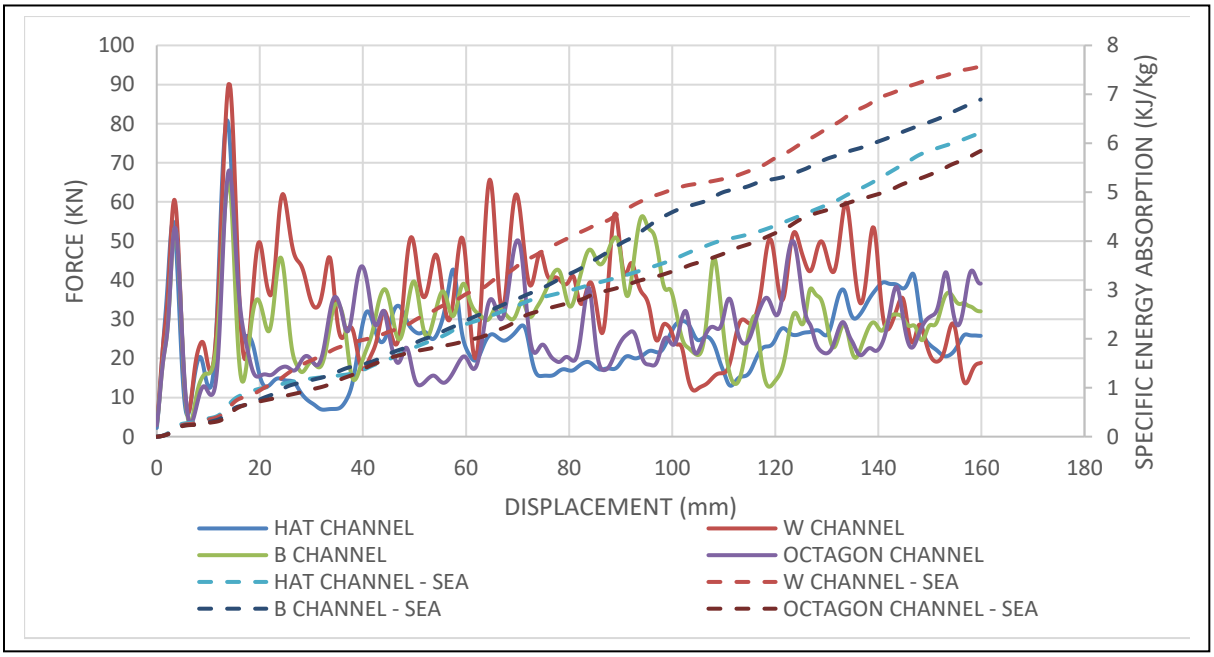

Figure 11: Layup 2 - force-displacement and specific energy absorption plots

Comparison of Energy absorption

From Figures 9 and 11, it is inferred that the replacement of 90° plies with two additional 0° plies in the stacking sequence (i.e., Layup 1) has a notable effect on the energy absorption. The impacting load is observed to have a decreasing trend with increasing the amount of fiber oriented at 45° and 90°. Moreover, results in Figure 12 show that the total SEA for each channel comprised of the $[\pm 45/0_2]_s$ laminate are higher in comparison to the $[0/\pm 45/90]_s$ laminate, and may be due in part to the fact that there are no plies oriented along the transverse direction. This variation is

principally a result of a higher lamina longitudinal compressive strength (X_c = 0.575 GPa) compared to the lamina transverse compressive strength (Y_c = 0.15 GPa). The position of plies along the axial direction creates a significant difference in crashworthiness metrics. Consequently, a decrease of 0° plies may reduce the axial stiffness of the composite structure. In addition, the position of the off-axis plies may also play a role in the SEA characteristics for the channels studied.

Moreover, the W channel specimen was intentionally developed with an increased number of edges, which seemed to influence the cracks that formed along the axial direction. This confirms that the additional splitting cracks in W channel led to higher energy absorption in both stacking sequences when compared to the other channels. The results show that the W channel specimens exhibited a high SEA of 8.5 and 7.4 KJ/Kg for Layup 1 and 2 respectively. This indicates that both the channel geometry and the laminate axial stiffness have a significant role in determining the specific energy absorption characteristics of CFRP channels.

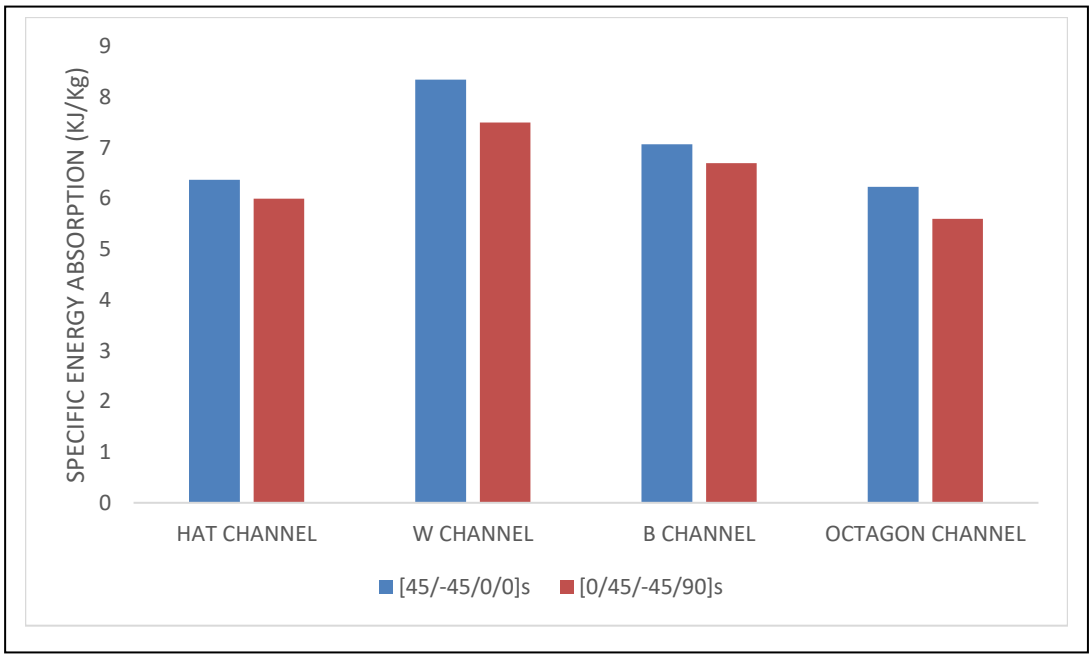

Figure 12: SEA comparison of two stacking sequence with four geometrical configurations.

Conclusions and Future work

The dynamic impact of axial crush channels comprised of unidirectional non-crimp fabric carbon fiber/epoxy composites has been numerically analyzed, and the effect of geometry and layup sequence on the specific energy absorption characteristics was investigated. The results indicate that the variation of geometry and stacking sequence has a significant effect on the specific energy absorption and impact load of composite structures. Comparative results indicate that the W channel has approximately 15% increased energy absorption in both layup sequences considered. However, having the 45° plies biased towards the outside and having a dominant number of 0° plies has relatively high specific energy absorption in all the channels. Nevertheless, the results of this study, represent an essential step towards numerical modeling and developing of automotive front lower rail with unidirectional non-crimp composites. Ongoing works include the experimental validation of the four straight channels in both quasi-static and dynamic conditions.

Acknowledgments

The authors would like to thank the Natural Sciences and Engineering Research Council of Canada (NSERC) for the financial support through Collaborative Research and Development Grant No. CRDPJ 507776 – 16, Ontario Centers of Excellence (OCE), Ontario Advanced Manufacturing Consortium (AMC), as well as sponsors Honda R&D Americas, Hexion Inc., Zoltek Corp. and LAVAL International.

Bibliography

1. Hull D. A unified approach to the progressive crushing of fiber-reinforced composite tubes. Comp Sci-Tech. 1991;40:377-421.
2. C. Fais, Lightweight automotive design with HP-RTM, Reinforc Plast 55 (Issue 5) (2011) 29-31.
3. COMPOSITES EUROPE highlights solutions for mass production of automotive composites, Reinforc Plast 55 (Issue 4) (2011) 45-46.
4. https://www.hexion.com/en-AU/applications/composites/automotive/structural/, Accessed date: 20 May 2019.
5. McGregor, Carla, Reza Vaziri, and Xinran Xiao. 2010. “Finite Element Modelling of the Progressive Crushing of Braided Composite Tubes under Axial Impact”. International Journal of Impact Engineering 37 (6). Elsevier BV: 662–72. doi:10.1016/j.ijimpeng.2009.09.005.
6. McGregor, Carla, Navid Zobeiry, Reza Vaziri, Anoush Poursartip, and Xinran Xiao. 2017. “Calibration and Validation of a Continuum Damage Mechanics Model in Aid of Axial Crush Simulation of Braided Composite Tubes”. Composites Part A: Applied Science and Manufacturing 95 (April). Elsevier BV: 208–19. doi:10.1016/j.compositesa.2017.01.012.
7. F. Deleo, B. Wade, P. Feraboli, P. Paolo, F. Uw, and M. R. B. R, “Crashworthiness of composite structures: experiment and simulation,” Am. Inst. Aeronaut. Astronaut., pp. 1–22, 2009.
8. Lukaszewicz DH-JA. Automotive Composite Structures for Crashworthiness. Elmarakbi A(ed). In: Advanced Composite Materials for Automotive Applications: Structural Integrity and Crashworthiness. Chichester, United Kingdom: Wiley, 2013.
9. Farley GL, Wolterman, R.L, Kennedy JM. The effects of crushing surface roughness on the crushing characteristics of composite tubes. J Am Helicopter Soc. 1992:July:53-60.
10. Hamada H, Coppola JC, Hull D, Maekawa Z, Sato H. Comparison of energy absorption on the carbon/epoxy and carbon/PEEK composite tubes.Composites. 1992;23(4):245-52.
11. Karbhari VM, Haller JE. Rate and architecture effects on the progressive crush of braided tubes. Comp Struct. 1998;43(2):93-108.
12. Mamalis AG, Manolakos DE, Demosthenous GA, Ioannidis MB. Analytical modeling of the static and dynamic axial collapse of thin-walled fiberglass composite conical shells. Int J Impact Eng. 1997;19(5):477-92.
13. A. Cherniaev, Y. Zeng, D. Cronin, and J. Montesano, “Quasi-static and dynamic characterization of unidirectional non-crimp carbon fiber fabric composites processed by HP-RTM,” Polym. Test., 2019.
14. Kalhor R, Case SW. The effect of FRP thickness on energy absorption of metal-FRP square tubes subjected to axial compressive loading. Compos Struct 2015;130:44-50.
15. Mahdi E, Hamouda AMS, Sebaey TA. The effect of fiber orientation on the energy absorption capability of axially crushed composite tubes. Mater Des 2014;56(4):923-8.
16. A. Cherniaev and J. Montesano, “Thin-Walled Structures Predicting the axial crush response of

CFRP tubes using three damage-based constitutive models," vol. 129, no. February, pp. 349–364, 2018.

17. Boria, S., J. Obradovic, and G. Belingardi. 2015. "Experimental and Numerical Investigations of the Impact Behaviour of Composite Frontal Crash Structures". Composites Part B: Engineering 79 (September). Elsevier BV: 20–27. doi:10.1016/j.compositesb.2015.04.016.
18. Suratkar A, Fan Y, Montesano J, Wood J. Quasi-static mechanical characterization of non-crimp carbon fiber reinforced epoxy laminates manufactured using HP-RTM process. SPE Automotive Composites Conference & Exhibition (ACCE), Novi, US, Sep 5-7, 2018.
19. LS-DYNA, ® Keyword user's manual volume II: material models, Livermore Software Technology Corporation (LSTC), 2013.
20. B. P. Bussadori, K. Schuffenhauer, and A. Scattina, "Modelling of CFRP crushing structures in explicit crash analysis," Compos. Part B Eng., vol. 60, pp. 725–735, 2014.